Published in final edited form as:
IEEE J Sel Top Quantum Electron. 2010 May ; 16(3): 545–554. doi:10.1109/JSTQE.2009.2033609.

Optical Microangiography: A Label Free 3D Imaging Technology to Visualize and Quantify Blood Circulations within Tissue Beds *in vivo*

Ruikang K Wang, Ph.D.
Department of Biomedical Engineering, School of Medicine, Oregon Health & Science University, 3303 SW Bond Avenue, Portland, OR 97239

Abstract

Optical microangiography (OMAG) is a recently developed volumetric imaging technique that is capable of producing 3D images of dynamic blood perfusion within microcirculatory tissue beds *in vivo*. The imaging contrast of OMAG image is based on the intrinsic optical scattering signals backscattered by the moving blood cells in patent blood vessels, thus it is a label free imaging technique. In this paper, I will first discuss its recent developments that use a constant modulation frequency introduced in the spectral interferograms to achieve the blood perfusion imaging. I will then introduce its latest development that utilizes the inherent blood flow to modulate the spectral interferograms to realize the blood perfusion imaging. Finally, examples of using OMAG to delineate the dynamic blood perfusion, down to capillary level resolution, within living tissues are given, including cortical blood perfusion in the brain of small animals and blood flow within human retina and choroids.

Keywords

Optical microangiography; Fourier domain optical coherence tomography; microcirculation; cerebral blood flow; neurological disease models; retinal blood flow

I. Introduction

Non-invasive and label free imaging techniques for quantifying blood flow - down to capillary-level resolution - are of great value for biomedical research, and clinical diagnostics and treatments for diseases that have vascular aetiology or involvement [1][2]. For example, accurate visualization of microvascular networks, and the quantification of tissue perfusion under normal and pathophysiologic conditions are critical in evaluating

(Phone: 503-418-9317; fax: 503-418-9311; wangr@ohsu.edu)..
Ruikang K. Wang is currently a professor of Biomedical Engineering, and a professor of Anesthesiology & Peri-Operative Medicine at Oregon Health & Science University. He gained his first degree and M.Sc. degree in Metrology from Tianjin University in 1988 and 1990, respectively. He obtained his Ph.D. degree in optical engineering from Glasgow University, Scotland in 1995. After 2 years postdoctoral research training at Glasgow, he was appointed as a lecturer and then senior lecturer in Bio-imaging Science at Keele Medical School, Stoke-on-Trent, UK. At the age of 36 years in 2002, Dr Wang became a chair professor in Biomedical Optics at Cranfield University, UK, where he created and directed Biophotonics and Imaging Laboratory. In 2005, Dr Wang moved to Oregon Health & Science University where he is currently the director of Biophotonics and Imaging Laboratory. Up to now, he has published more than 120 peer reviewed journal articles, one monograph in optical information processing, as well as 7 book chapters. His current research interests include optical coherence tomography, optical micro-angiography, optics in tissue engineering, and photon propagations in biological tissues. Dr Wang is currently a member of Optical Society of America (OSA) and the international Society of Photo-Instrumentation Engineers (SPIE).

This potential conflict of interest has been reviewed and managed by OHSU.

existing and emerging therapeutic strategies to treat neurovascular diseases [3]-[7], such as ischemic and hemorrhagic stroke, TBI, vascular dementia, inflammation, and some seizure disorders, and to develop potential drugs to support or limit neovascular growth, e.g., angiogenesis [8]-[10], such as in the treatment of cancers. In these situations, it would be useful to localize microstructural features of tissue and blood flow that supplies the perfused tissue - and to do so at user-specified discrete spatial locations in either the superficial or deep tissues, without invasion of any kind.

Important limitations still remain in imaging functional blood perfusion with current techniques. Such limitations include their invasiveness (e.g., radioactive methods), their inability to provide 3D information (e.g., laser speckle imaging), their inability to provide adequate spatial and temporal resolutions (e.g., MRI), and their inability to image beyond shallow (>300 μm) depths (e.g., confocal microscopy). What is needed is a real time, label-free, and non-invasive imaging technique that is capable of measuring 3D morphological and functional parameters of blood perfusion in tissue, at high resolution (e.g., <10 μm). With such a technique, the detailed, functional architecture of the perfused microvascular network can be revealed; the volumetric rheology and perfusion status can be quantified.

Optical microangiography (OMAG) is a recently developed novel imaging technique that produces 3D images of dynamic blood perfusion within micro-circulatory tissue beds at an imaging depth up to 2.0 mm [11]-[16]. OMAG produces imaging contrasts via endogenous light scattering from moving particles (e.g., flowing blood cells within open vessels), thus, no exogenous contrast agents are necessary; hence, OMAG is label-free. OMAG has its origin in Fourier domain optical coherence tomography (FDOCT) [17][18], but is an improvement over FDOCT and Doppler OCT (DOCT) [19][20] through its innovative spatial frequency analysis of the time-varying spectral interferograms [11]-[16]. This spatial frequency analysis allows OMAG to separate signals that are backscattered by moving particles (e.g., blood cells), from signals that are backscattered by static particles (e.g. bulk tissue). The result is high-resolution mapping of dynamic blood perfusion at capillary-level resolution. In essence, OMAG mathematically maps the backscattered optical signals from the moving particles into one image - that is, the blood flow image - while it *simultaneously* maps the backscattered optical signals from the static particles into a second image, which is the microstructural image. These distinct features of OMAG provide us a unique ability to perform comprehensive measurements of the morphological and functional parameters of blood perfusion within a scanned tissue volume.

The development of OMAG was first originated from the development of ultrafast full range complex FDOCT imaging of *in vivo* tissue sample [21]-[23], in which a constant modulation frequency was introduced into the OCT spectral interferograms to achieve full range complex imaging without limitation on the imaging speed. It was then quickly realized that this introduction of a constant frequency modulation in the spectral interferogram lends itself to separate the optical signals backscattered by the moving blood cells from the optical signals backscattered by the tissue background, i.e., tissue microstructures, thus the possibility to delineate the functional blood flows in 3D within a living tissue sample [11]. The first OMAG system used the moving reference mirror that was mounted onto a piezo translational stage to introduce the required constant frequency modulation in the spectral interferograms to achieve the blood flow imaging [11][12], including directional flow [13][14]. It was later discovered that the spatial frequency modulation can be introduced by an offset of the scanning probe beam on the scanning mirror in the sample arm that is used to scan the probe beam over the sample [15][23]. This is advantageous because the required modification of FDOCT system to provide OMAG capability is minimal, and moreover, the mechanical movement of piezo stage to drive the reference mirror to move at a constant speed is avoided, thus both cost effective and ease of implementation.

The most recent development of OMAG relies on the blood flow inherent within the patent blood vessels to modulate the spectral interferograms so that the optical scattering signals from the moving blood cells and static scatters can be effectively separated [16]. Because of its use of the Doppler frequency induced by the blood flow to modulate the spatial interferograms, neither hardware nor software approaches are necessary in its implementation. In this paper, we will discuss the basic operation principles behind this latest version of OMAG. And then the examples to show the potentials of OMAG imaging of dynamic cerebral blood flow, down to capillary level resolution, within cortex in mice with the skull left intact are given.

II. Optical Micro-angiography: Theoretical Aspects

OMAG is a functional extension to the recently developed Fourier Domain OCT, which can provide micro-structural and blood flow images of the scanned tissue sample in parallel. The most recent development of OMAG essentially uses Fourier filtering to separate the optical signals backscattered by the blood cells moving within patent blood vessels from the optical signals backscattered by the static micro-structures of tissue sample, and uses Hilbert transformation to discriminate the directions of the moving blood cells relative to the incident probe beam direction.

In FDOCT, the spectral interference signal formed between the reference light and the light backscattered from a sample is detected by an ultrahigh speed spectrometer, where a line scan CCD camera receives the dispersed optical signal. The mathematical expressions for the spectral interference signal detected by each pixilated detector on the camera are essentially the same except the wavelength, λ. We assume the wavenumbers of a broadband light source are from k_0 to $k_0 + \Delta k$, where $k_0 = 2\pi/\lambda_0$, and these wavenumbers cover N pixels of the line scan camera. As a consequence, the spectral interference signal detected by each pixel can be written as a function of k_i $(i = 1, 2, \ldots N)$,

$$I(k_i) = S(k_i)\left\langle \left| E_R \exp(j2k_i r) + \int_{-\infty}^{\infty} a(z) \exp\{j2k_i[r+nz]\}\, dz \right|^2 \right\rangle \quad (1)$$

where ●> denotes the time average , $j = \sqrt{-1}$, k_i is the wavenumber of the light captured by the ith detector (pixel) of the camera, $I(k_i)$ is the light intensity captured by the ith detector, $S(k_i)$ is the spectral density of the light source at k_i, r is the optical path length for the light traveled in the reference arm, n is the refractive index of the sample, $a(z)$ is the magnitude of the light backscattered at depth z. In most FDOCT systems, the imaging is achieved by scanning the probe beam on the sample frame by frame, i.e., B scan mode. So, the signal captured by the ith pixel in each B-scan can be written as a function of time variable t that relates to the position of focus beam spot on the sample,

$$I(k_i, t) = S(k_i)\left\langle \left| E_R \exp(j2k_i r) + \int_{-\infty}^{\infty} a(z,t) \exp\{j2k_i[r+nz]\}\, dz \right|^2 \right\rangle \quad (2)$$

Because the light backscattered from the sample is quite weak compared to the light reflected from the reference mirror, we do not consider the self cross-correlation between the light backscattered from different positions within the sample. We also do not consider the DC signals because they do not contribute to useful FDOCT/OMAG signals. In these cases, Eq. (2) can be written as:

$$I(k_i,t) = 2S(k_i)E_R\int_{-\infty}^{\infty} a(z,t)\cos(2k_i nz)\,dz \tag{3}$$

The spatial frequency analysis of $I(k_i,t)$ against t can be performed by Fourier transformation, i.e.,

$$I(k_i,f) = FT[I(k_i,t)]|_t \tag{4}$$

It is clear that Eq. (3) is constant if the sample is totally optically homogeneous, which means that $a(z,t)$ and n do not vary within the entire sample. If this is the case, then the spatial frequency components of the sample in lateral direction presented by Eq. (4) will be a delta function, shown as a red arrow in Fig.1 (A). However in real situations, our imaging sample is often optically heterogeneous, which means that $a(z,t)$ and n are functions of time variable t. Thus, Eq. (3) needs to be expressed as:

$$I(k_i,t) = 2S(k_i)E_R\int_{-\infty}^{\infty} a(z,t)\cos(2k_i n(z,t)z)\,dz \tag{5}$$

As a consequence, Eq. (5) is not constant anymore. The intensity captured by the CCD camera will be modulated by the heterogeneous properties of the sample along each B-scan. The spatial frequency components of a static tissue sample, which we call the heterogeneous frequencies, will exhibit as a randomly distributed function around zero frequency with a bandwidth of BW, as shown in red curve in Fig. 1(B) [22].

When there is a patent blood vessel buried within a motionless tissue at position (z_1,t_1), we assume the blood cells (scattering particles) within the vessel move towards/away the incident beam at a velocity v. The frequency of the light backscattered from these blood cells will be modulated by its velocity. Then, Eq. (5) can be expressed as:

$$I(k_i,t) = 2S(k_i)E_r \left[\int_{-\infty}^{\infty} a(z,t)\cos(2k_i n(z,t)z)\,dz + a(z_1,t_1)\cos[2k_i n(z_1,t_1)(z_1 - vt)]\right] \tag{6}$$

Here we also do not consider the self cross-correlation signal from within the sample. The 1st term on the right side of Eq. (6) represents backscattering signals from a static sample with reflectivity of $a(z,t)$, while the 2nd term represents backscattering from the moving particles with reflectivity of $a(z_1,t_1)$ with a velocity of v at position (z_1,t_1). Moving particles produce an optical frequency shift caused by the well known Doppler effect. In other words, the moving particles would modulate the spectral interferograms through a Doppler beating frequency at all the wavelengths covered by the bandwidth of light source used. When the particle velocity is large enough, its Doppler beating frequency will shift the moving frequency components away from the heterogeneous band width in the spatial frequency domain, i.e., $I(k_i, f)$. This is illustrated in Fig.1 (C), the blue curve is the Doppler beating frequency part.

With an appropriate selection of frequency $f_c = BW/2$, three functions can be constructed:

$$I(k_i,f)_{\text{structure}} = \begin{cases} I(k_i,f), & \text{when} \quad f<|f_c| \\ 0, & \text{elsewhere} \end{cases} \tag{7}$$

$$I(k_i, f)_{\text{Flow}} = \begin{cases} I(k_i, f), & \text{when} \quad f > |f_c| \\ 0, & \text{elsewhere} \end{cases} \tag{8}$$

$$I(k_i, f)_{\text{DFlow}} = \begin{cases} I(k_i, f), & \text{when} \quad f > f_c, \text{or} f < -f_c \\ 0, & \text{elsewhere} \end{cases} \tag{9}$$

Taking an inverse Fourier transformation and considering the symmetrical property, Eq.(7) would become the same as Eq. (5), that represents the optical signals backscattered by the static scattering elements from the sample, i.e., microstructures. Eq. (8) becomes,

$$I(k_i, t)_{\text{Flow}} = 2S(k_i) E_R a(z_1, t_1) \cos[2k_i n(z_1, t_1)(z_1 - vt)], \tag{10}$$

Eq. (10) represents the optical signals backscattered by the moving particles, e.g., moving blood cells within tissue sample, but without discrimination of the directions of the moving particles. Here the microstructural signals have been eliminated.

However, the result for inverse Fourier transform of Eq. (9) will be:

$$I(k_i, t)_{\text{DFlow}} = 2S(k_i) E_R \quad a(z_1, t_1)[\cos[2k_i n(z_1, t_1)(z_1 - vt) - j\sin[2k_i n(z_1, t_1)(z_1 - vt)] \tag{11}$$

when $v>0$ (i.e., the particles moving towards the incident probe beam direction). Whereas when $v<0$ (i.e., the particles moving away from the incident probe beam direction), Eq. (11) becomes:

$$I(k_i, t)_{\text{DFlow}} = 2S(k_i) E_R \quad a(z_1, t_1)[\cos[2k_i n(z_1, t_1)(z_1 - vt) - j\sin[2k_i n(z_1, t_1)(z_1 - vt)] \tag{12}$$

Mathematically, Eq. (12) is clearly the complex conjugate of Eq. (11). Therefore, according to Ref [11], the directional blood flow is discriminated. The optical signals that represent the particles moving towards the probe beam will situated at the positive output plane of OMAG, while those from the particles moving away from the probe beam direction will be located at the negative plane.

As a consequence, OMAG will provide following images of the scanned tissue sample in parallel: 1) microstructural image, 2) flow image without directional information, and 3) directional flow image.

III. OMAG System Setup

The system used to obtain the OMAG imaging results in this paper is illustrated in Fig.2. A superluminecent diode (SLD, DenseLight, Singapore) with a central wavelength of 1310 nm and a spectral bandwidth of 56 nm was used as the light source, which provided an axial imaging resolution of ~13 μm in air. The light from the SLD was coupled into a fiber-based Michelson interferometer, via an optical circulator. In the reference arm, the light was delivered onto a stationary mirror; and in the sample arm, the light was focused into a sample via an objective lens. The zero delay line of the system was set at ~0.5 mm above the

focus spot of sample beam. With a 50 mm focal length of the objective lens in the sample arm, the size of the focus spot on the sample was ~16 μm, i.e., the lateral resolution of the system was ~16 μm. The light backscattered from the sample and reflected from the reference mirror were recombined by a 2×2 optical fiber coupler, and then was routed to a home-built high speed spectrometer via the optical circulator. The spectrometer consisted of a collimator of 30 mm focal length, a 1200 lines/mm transmitting grating, an achromatic lens with 100 mm focal length and a 14-bit, 1024 pixels InGaAs line scan camera. The maximum line scan rate of the camera was ~47 KHz. This spectrometer setup had a designed spectral resolution of 0.141 nm, which gave a measured imaging depth of ~3.0 mm on the each side of the zero delay line.

To achieve 3D imaging, an x-y galvo-scanner was used to raster-scan the focused beam spot across the sample, with one scanner for X-direction (lateral) scan, and another for Y-direction (elevational) scan. For the experiments presented in this study, the camera integrating time was set at 31 μs for imaging, allowing 1 μs for downloading the spectral data from CCD (1024 pixels, A scan) to the host computer via CameraLink™ and a high-speed frame grabber board (PCI 1428, National Instruments, USA). This configuration determined a line scan rate of ~31 KHz for the camera. The imaging rate was set at 20 frames (B scan) per second (fps). Each B scan had 2.5 mm span over the sample, consisting of 1500 A-lines. This represents an over sampling factor of ~10 because the lateral resolution of the system is ~16 μm. The minimal blood flow velocity that can be detected with these configurations was empirically determined to be ~200 μm/s. In the elevational direction, there were 500 discrete points along ~2.5 mm, i.e., 500 B scans. Hence the data cube of each 3D image (C scan) was composed of 1024 by 1500 by 500 (z-x-y) voxels, which took ~25 s to acquire. The operations for probe beam scanning, data acquisition, data storage and hand-shaking between them were controlled by a custom software package written in C++ language. Note that 500 B scans for a C scan represented over sampling in the elevational direction. In practice, however, 200 B scans would be sufficient to obtain the volumetric images, leading to a temporal resolution of ~10 s for 3D OMAG imaging using the current setup

IV. Results and Discussions

A. OMAG Shows Detailed Cerebrovascular Perfusion in Live Mice with Cranium Left Intact

Quantifying 3D CBF in individual vessels and tissues of small animals has proven invaluable in understanding mechanisms of human cerebrovascular diseases and brain metabolisms. Previous studies have used OMAG for high resolution transcranial imaging of blood flow in the cerebral cortex in mice without a need to remove or thin the cranium [11]-[16]. During the experiment prior to OMAG imaging, the mouse was anesthetized and mounted on a custom-built stereotaxic stage for stabilization. The skin over cranium was incised and carefully pulled apart to expose the bone and to create a window for OMAG imaging. Then, the OMAG system as described in Fig. 2 was used to progressively slice the mouse brain through cranium in order to collect 3D raw spectral interferogram dataset.

Figure 3 shows the OMAG output obtained from the raw optical spectrograms, representing one slice within the 3D dataset. Figure 3(A) gives the cross-sectional microstructural image of the scanned tissue slice, representing the optical signals backscattered by the static scattering elements. This image is identical to the conventional OCT image within which the histologically important layers, such as cranium and gray matter, are clearly demarcated. However, it does not reveal blood flow information. Because red blood cells move through all open blood vessels, such as capillaries, the blood flows can be localized by OMAG (Fig. 3B). Since Figs. 3(A) and 3(B) are mirrored in OMAG, they could be fused into a single image so that flowing blood can be precisely localized within the tissue sample. The

structural and blood flow images were obtained in parallel, which is one of the advantages offered by OMAG. Figure 3(C) indicates that the current OMAG system is capable of imaging blood flowing in capillaries. The 1310nm OMAG system resolved cortical structures and localized blood flow at depths of ~2.0 mm, an imaging depth that cannot be achieved with confocal microscopy. Similar results were obtained using an 840nm wavelength OMAG system [11].

Because of OMAG's fast imaging speed, 3D data set of raw spectral interferograms can be collected by scanning the probe beam in x-y direction in the OMAG system. After evaluating the spectrogram data slice by slice, the processed slices can be re-combined and aligned to yield the 3D volume OMAG images. Fig. 4 gives the imaging results obtained from a cortical tissue volume of $2.2\times2.2\times1.7mm^3$ in a live mouse brain with the cranium intact, while imaging time was less than ~25 sec. The microvascular blood perfusion was clearly delineated and localized within the tissue volume. With this 3D volume data set, we were able to separately identify blood perfusion in the skull bone, meninges, and the brain cortex, as shown in Figs. 4(E) and 4(F). These images clearly demonstrate the feasibility of OMAG to assess the morphological parameters of the blood vessels that innervate the perfused tissue, including vessel diameters, vessel density, and the volume of blood flowing in vessels.

To obtain *quantitative* blood flow information, we have further advanced OMAG by combining the laser Doppler velocimetry technique with OMAG, i.e., Doppler OMAG (DOMAG), so that the blood flow velocities in the functional vessels can be quantified within the scanned tissue [16]. Figure 5 (shown as projection images onto x-y) illustrates the ability of OMAG to quantitatively image CBF in mice through the intact cranium. Color in this figure distinguishes flows toward and away from the incident probe-beam direction. These results indicate that DOMAG (Fig.5B) can determine the velocities of blood flows within all vessels in the scanned tissue.

B. OMAG Offers Opportunity to Examine Cerebral Blood Perfusion Changes Globally and in Individual Vessels over Cortex in Mice

3D OMAG provides detailed information about blood flow in both tissue volumes and individual blood vessels. OMAG thus may be a useful tool for the investigation of diseases, where changes in blood perfusion play an important role in etiology, pathogenesis, prognosis, or response to treatments. For example, characterization of cortical perfusion during experimental focal cerebral ischemia in mice may help us better understand the pathophysiology of acute thrombotic ischemic stroke and shed light on the mechanism of selected pharmacological interventions. In these situations, it would be desirable to examine the cerebral blood perfusion changes globally and in individual vessels over the cortex in order to understand how the brain functions to regulate the blood flow to compensate the focal insult. To evaluate whether OMAG can serve as a useful tool in characterizing cerebrovascular blood flow over the entire cortex, multiple 3D images of the mouse brain were collected over different regions of the skull. Images from different regions were then combined as a mosaic, and displayed with and without the directional flow velocity information (Fig.6). The striking OMAG imaging results provided volumetric measurements of detailed blood perfusion through the cerebrovascular tree down to the capillary level with the skull left intact, without the need for dye injection, contrast agents, or surgical craniotomy. 3D vascular perfusion map obtained by OMAG had an excellent agreement with that from direct photographing of blood vessels on the surface of the cerebral cortex.

These results suggest that OMAG maybe feasible to monitor changes in flow direction, volume, and opening or closing/occlusion of small to large vessels in the entire cerebral cortex of mice. We thus investigated how temporary placement of an occlusive filament into

the middle cerebral artery (MCA) affects blood perfusion distribution in the brain using an established model of experimental acute thrombotic ischemic stroke (ATIS) in mice [24]. This disease model has been extensively characterized in several laboratories, and has been used and validated for the development of new treatments for stroke, e.g., [25]-[29]. In our preliminary phase of study, stroke was induced in mice by MCA occlusion (MCAO) using the intraluminal filament technique followed as described by Eliason et al [24] and modified in [25], and OMAG imaging was used to obtain 3D dynamic cerebrovascular perfusion images before, during and after MCAO for up to 24 hr. The OMAG image showed major, apparently bilateral changes in the cerebral microcirculation following placement of the filament into the MCA for 60 min [Fig. 7(B)] as compared to the control, i.e. baseline [Fig. 7(A)]. The occlusion induced by the foreign body in the major blood vessel caused immediate focal disappearance of several flow patterns as well as redirection of flow in other parts of the brain. Some occlusions were temporary, as suggested by reappearance of flow following removal of the filament from the MCA at 60 min. However, some vessels that had flow at baseline (before MCAO) remained hypoperfused or outright ischemic, and several occlusions seem to have persisted even one day after removal of the filament from the MCA [Fig. 7(C)]. This suggested progressive development of an occlusive component in the model following placement the foreign body in the MCA. The data were consistent with progressively spreading thrombotic occlusions, as documented on histopathology in the same model by other laboratories, e.g., [25].

The fact that OMAG images through bone, in contrast to confocal microcopy [30] and laser speckle imaging [31], is useful for obtaining functional information about tissue perfusion. The minimally invasive nature of OMAG also allows for sustained and repeated imaging of the sample, which is important in order to track the changes of CBF as they may occur in the cases of thrombosis, recanalization and angiogenesis.

C. OMAG Images the Blood Perfusion within Human Retina and Choroids

The most recent development in imaging the ocular blood perfusion in humans is to use phase resolved Doppler OCT (PR-DOCT) [19][32]. PRDOCT uses optical phases in the interference signals to evaluate the blood flow. However, the use of optical phases is very sensitive to the sample movement, optical heterogeneity of tissue, and the strength of OCT signals. The noise production makes it difficult for PR-DOCT to image ocular blood flow, particularly in small blood vessels. In contrast to PR-DOCT, OMAG does not directly rely on phase information of the OCT signals to visualize blood flow, implying that the noise production originating from the inevitable sample movement and the optical heterogeneity of sample is kept at minimum. Therefore, it is expected that OMAG would outperforms DOCT in imaging the blood flows in human retina and choroids.

Figure 8 shows the *in vivo* OMAG imaging results captured at a position near to the optic disk from a volunteer. Figure 8(A) gives the OCT fundus projection image obtained by integrating signals along the depth direction from the volumetric OCT/OMAG structural images using the method proposed by Jiao *et al* [33], where the major blood vessels over the retina can be seen, but not in the choroid. Figure 8(B) represents one cross-sectional image within the volumetric OCT image at the position marked by the yellow line in Fig. 8(A). Figure 8(C) is the corresponding blood flow image, where it can be seen that the blood flows within the retina and choroidal layers are clearly delineated. In the retinal region, not only some big vessels, but also the capillary vessels are presented. Although the blood flows in the vessels in the choroid region are slow, which are difficult to be detected by PRODT, they can be captured by OMAG imaging method.

Because OMAG gives the volumetric structural and flow images simultaneously, the 3D vasculatures can be merged into the 3D structural image. Such merged volumetric image is

illustrated in Fig. 8(D), where a cut-through view in the center of volumetric structural image is used to better appreciate how the blood vessels innervate the tissue. To separately view the blood vessels within the retina and choroidal layers, the blood flow signals within the retina and choroid are coded with green color and red color. The result is shown in Fig. 8(E), where the flow image shows us two vessel networks with good connection between vessels.

Figure 9(A) gives the x-y projection image with the blood vessels in retina coded with green color and those in choroids with red color. Figure 9(B) and Fig. 9(C) illustrate the x-y projection images produced from blood vessels in retina and choroids, separately.

All of these results demonstrate that OMAG delivers superior imaging performance, not only in retina, but also in choroids, including the capability of imaging capillary vessels. However, it is noted that when compared to the imaging results obtained from the animal brain shown in the previous sections, the capillary blood flows are less evident in the human retina. There may be a number of reasons for this observation: 1) there is inevitable, severe motion in human retina imaging. Currently the motion artifacts are minimized by phase-compensation evaluated from the bulk tissue movement through PRDOCT method [15]. The phase compensation may mask the capillary blood flow. Therefore, a better approach than the current phase compensation method is needed to improve the OMAG performance in imaging the capillary blood flows within the human retina. And 2) the capillary vessel density in human retina may be less than in the animal brain.

V. Conclusion

We have discussed a label-free optical microangiography technique capable of high resolution imaging of blood perfusion within localized blood vessel embedded within highly scattering tissue. By exploiting the optical scattering signal properties of the FDOCT interferograms, the moving and static scattering elements within tissue can be efficiently separated, thereby enabling precise localization of blood perfusion in 3-dimensional microstructures. Although the current paper demonstrated the label-free capability of OMAG imaging of blood perfusion, the use of contrast agents and newer imaging agents administered into blood, for example nanoparticles and microbubbles [34] may offer a potential to increase the light backscattered from the moving elements, thus enhancing further the sensitivity of 3-D OMAG. The system is compact, fast, optically stable, and easily implemented in both the hospital and research laboratory environments.

Although the present report demonstrates the usefulness of OMAG in transcranial cerebrovascular imaging in mice models and in imaging ocular blood flow in humans, it is also well suited for performing 3-D angiograms on thick tissues in other basic and clinical settings, where the visualization and quantification the microcirculation are important for understanding mechanisms and treatments, e.g. tumor angiogenesis, wound healing. Other examples of prospective applications include neuroscience, where changes in cortical blood flow are coupled to certain types of neuropathology, such as stroke, traumatic brain injury, hemorrhage and dementia; ophthalmology, where ocular and retinal circulatory beds are very important in the diagnosis and management of disorders such as glaucoma, diabetic retinophathy and age-related macular degeneration. As OMAG and the associated computation are developed into a rapid imaging system, we will be able to assess tissue perfusion at the resolution level of capillary flow in real time without interfering with the sample in a significant way.

Acknowledgments

The author acknowledges the contributions from his group members (Lin An, Sawan Hurst, Yali Jia, Zhenhe Ma, Hrebesh Molly Shadbush and Yaguang Zeng) for assisting the experiments using small animals, and his collaborators at OHSU (Nabil Alkayed, Andras Gruber, Mary Heinricher, and Alfred Nuttall) for discussions of the results presented in this paper. OptoVue has licensed technology from OHSU of which Dr. Wang is an inventor. The technology is used in this research, which however did not receive support from OptoVue.

This work was supported in part by research grants from the National Heart, Lung, and Blood Institute (R01 HL093140), National Institute of Biomedical Imaging and Bioengineering (R01 EB009682), National Institute of Deafness and other Communication Disorders (R01 DC010201) and the American Heart Association (0855733G). The content is solely the responsibility of the authors and does not necessarily represent the official views of grant giving bodies.

References

[1]. Yamada E, Matsumura M, Kyo S, Omoto R. Usefulness of a prototype intravascular ultrasound imaging in evaluation of aortic dissection and comparison with angiographic study, transesophageal echocardiography, computed tomography and magnetic resonance imaging. Am J. Cardiol 1995;75:161–171. [PubMed: 7810493]

[2]. Misgeld T, Kerschensteiner M. *In vivo* imaging of the diseased nervous system. Nature Rev. Neurosci 2006;7:449–463. [PubMed: 16715054]

[3]. Molina CA, Saver JL. Extending reperfusion therapy for acute ischemic stroke: emerging pharmacological, mechanical, and imaging strategies. Stroke 2005;36:2311–20. [PubMed: 16179577]

[4]. Albers GW, Amarenco P, Easton JD, Sacco RL, Teal P. Antithrombotic and thrombolytic therapy for ischemic stroke. Chest 2004;126S:483–512. the Seventh ACCP Conference on Antithrombotic and Thrombolytic Therapy.

[5]. Fisher M, Fernandez JA, Ameriso SF, Xie D, Gruber A, Paganini-Hill A, Griffin JH. Activated protein C resistance in ischemic stroke not due to factor V arginine506-->glutamine mutation. Stroke 1996;27:1163–6. [PubMed: 8685921]

[6]. Malonek D, Dirnagl U, Lindauer U, Yamada K, Kanno I, Grinvald A. Vascular imprints of neuronal activity: relationships between the dynamics of cortical blood flow, oxygenation, and volume changes following sensory stimulation. Proc. Natl. Acad. Sci. USA 1997;94:14826–14831. [PubMed: 9405698]

[7]. Hossmann K. Viability thresholds and the penumbra of focal ischemia. Ann Neurol 1994;36:557–565. [PubMed: 7944288]

[8]. McDonald, Choyke. Imaging of angiogenesis: from microscope to clinic. Nat. Med 2003;9:713–725. [PubMed: 12778170]

[9]. Padera TP, Stoll BR, So PT, Jain RK. Conventional and high speed intravital multiphoton laser scanning microscopy of microvasculature, lymphatics, and leukocyte-endothelial interactions. Mol. Imaging 2002;1:9–15. [PubMed: 12920856]

[10]. Jain RK. Delivery of molecular medicine to solid tumors: lessons from in vivo imaging of gene expression and function. J. Control. Release 2001;74:7–25. [PubMed: 11489479]

[11]. Wang RK, Jacques S, Ma Z, Hurst S, Hanson S, Gruber A. Three dimensional optical angiography. Optics Express 2007;15:4083–4097. [PubMed: 19532651]

[12]. Wang RK, Hurst S. Mapping of cerebrovascular blood perfusion in mice with skin and cranium intact by Optical Micro-AngioGraphy at 1300nm wavelength. Optics Express 2007;15:11402–11412. [PubMed: 19547498]

[13]. Wang RK. Three dimensional optical angiography maps directional blood perfusion deep within microcirculation tissue beds in vivo. Physics in Medicine and Biology 2007;52:N531–N537. [PubMed: 18029974]

[14]. Wang RK. Directional blood flow imaging in volumetric optical micro-angiography achieved by digital frequency modulation. Optics Letters 2008;33(16):1878–1880. [PubMed: 18709119]

[15]. An L, Wang RK. *In vivo* volumetric imaging of vascular perfusion within human retina and choroids with optical micro-angiography. Optics Express 2008;16:11438–11452. [PubMed: 18648464]

[16]. Wang RK, An L. Doppler optical micro-angiography for volumetric imaging of vascular perfusion in vivo. Optics Express 2009;17(11):8926–8940. [PubMed: 19466142]

[17]. Fercher AF, Drexler W, Hitzenberger CK, Lasser T. Optical Coherence Tomography - Principles and Applications. Rep. Prog. Phys 2003;66:239–303.

[18]. Tomlins PH, Wang RK. Theory, development and applications of optical coherence tomography. J Phys. D: Appl. Phys 2005;38:2519–2535.

[19]. Chen ZP, Milner TE, Srinivas S, et al. Noninvasive imaging of in vivo blood flow velocity using optical Doppler tomography. Opt. Lett 1997;22:1119–1121. [PubMed: 18185770]

[20]. Makita S, Hong Y, Yatagai MYT, Yasuno Y. Optical coherence angiography. Opt. Express 2006;14:7821. [PubMed: 19529151]

[21]. Wang RK. In vivo full range complex Fourier domain optical coherence tomography. Applied Physics Letters January;2007 90(5):054103.

[22]. Wang RK. Fourier domain optical coherence tomography achieves full range complex imaging in vivo by introducing a carrier frequency during scanning. Physics in Medicine and Biology 2007;52:5897–5907. [PubMed: 17881807]

[23]. An L, Wang RK. Use of scanner to modulate spatial interferogram for in vivo full range Fourier domain optical coherence tomography. Optics Letters 2007;32:3423–25. [PubMed: 18059954]

[24]. Eliason MJL, Sampei K, Mandir AS, Hurn PD, Traystman RJ, Bao J, Pieper A, Wang ZQ, Dawson TM, Snyder SH, Dawson VL. Poly (ADP-ribose) polymerase gene disruption renders mice resistant to cerebral ischemia. Nat Med 1997;3:1089–95. [PubMed: 9334719]

[25]. Shibata M, Kumar SR, Amar A, Fernandez JA, Hofman F, Griffin JH, Zlokovic BV. Anti-inflammatory, antithrombotic, and neuroprotective effects of activated protein C in a murine model of focal ischemic stroke. Circulation 2001;103:1799–805. [PubMed: 11282913]

[26]. Kilic E, Hermann DM, Hossmann KA. Recombinant tissue plasminogen activator reduces infarct size after reversible thread occlusion of middle cerebral artery in mice. NeuroReport 1999;10:107–11. [PubMed: 10094143]

[27]. Sawada M, Alkayed NJ, Goto S, Crain BJ, Traystman RJ, Shaivitz A, Nelson RJ, Hurn PD. Estrogen receptor antagonist ICI182,780 exacerbates ischemic injury in female mouse. J Cereb Blood Flow Metab 2000;20:112–8. [PubMed: 10616799]

[28]. Choudhri TF, Hoh BL, Prestigiacomo CJ, Huang J, Kim LJ, Schmidt AM, Kisiel W, Connolly ES Jr, Pinsky DJ. Targeted inhibition of intrinsic coagulation limits cerebral injury in stroke without increasing intracerebral hemorrhage. J Exp Med 1999;190:91–9. [PubMed: 10429673]

[29]. Tabrizi P, Wang L, Seeds N, McComb JG, Yamada S, Griffin JH, Carmeliet P, Weiss MH, Zlokovic BV. Tissue plasminogen activator (tPA) deficiency exacerbates cerebrovascular fibrin deposition and brain injury in a murine stroke model: studies in tPA-deficient mice and wild-type mice on a matched genetic background. Arterioscler Thromb Vasc Biol 1999;19:2801–6. [PubMed: 10559029]

[30]. Misgeld T, Kerschensteiner M. In vivo imaging of the diseased nervous system. Nat. Rev. Neurosci 2006;7:449–463. [PubMed: 16715054]

[31]. Dunn AK, Bolay H, Moskowitz MA, Boas DA. Dynamic Imaging of Cerebral Blood Flow Using Laser Speckle. J. Cereb. Blood Flow Metab 2001;21:195–201. [PubMed: 11295873]

[32]. White BR, Pierce MC, Nassif N, et al. In vivo dynamic human retinal blood flow imaging using ultra-high-speed spectral domain optical Doppler tomography. Opt. Express 2003;11:3490–3497. [PubMed: 19471483]

[33]. Jiao S, Knighton R, Huang X, Gregori G, Puliafito CA. Simultaneous acquisition of sectional and fundus ophthalmic images with spectral-domain optical coherence tomography. Opt. Express 2005;13:444–452. [PubMed: 19488371]

[34]. Lindner JR. Microbubbles in medical imaging: current applications and future directions. Nat. Rev. Drug Discov 2004;3:527–532. [PubMed: 15173842]

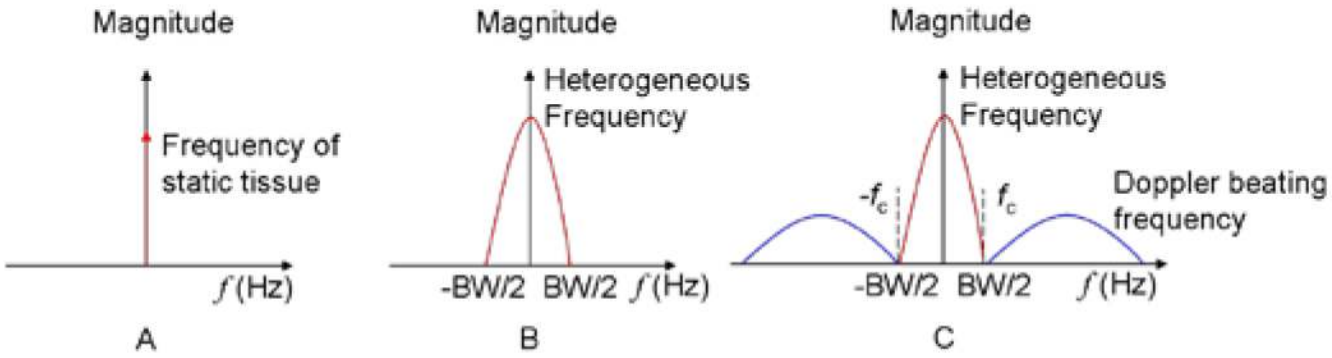

Fig.1.

Diagram of frequency components for different tissue sample: (A) an ideal tissue sample (optically homogeneous sample) with no moving particles; (B) a real tissue sample (optically heterogeneous sample) with no moving particles; (C) a real tissue sample (optically heterogeneous sample) with moving particles.

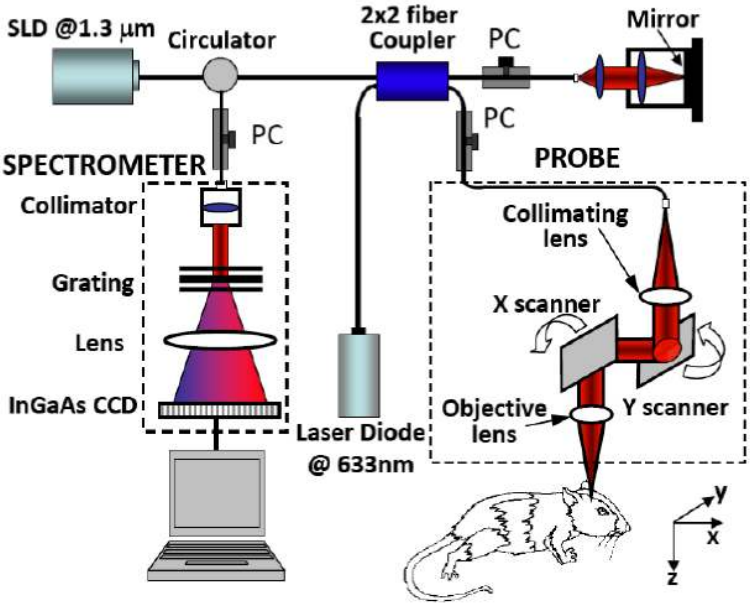

Fig.2.

Schematic of the OMAG system used in this study to image the velocities of blood flow, where PC represents the polarization controller and CCD the charged coupled device. The laser diode emitting the light at 633 nm was used for aiming purposes during imaging.

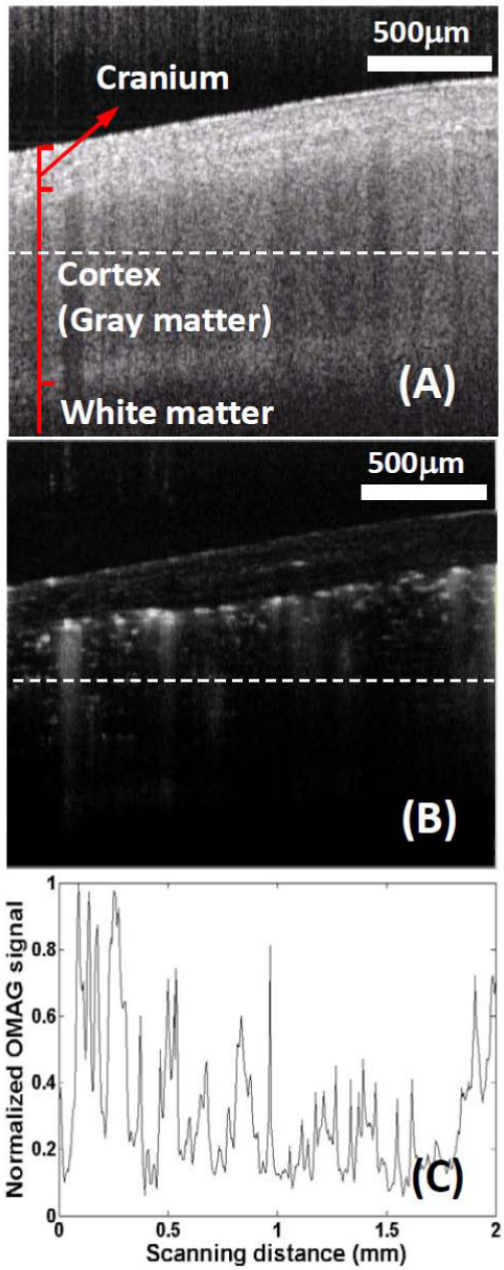

Fig.3.

2D imaging of cerebral cortex in mice. (A) OMAG structural image, (B) corresponding OMAG blood flow image where abundant functional capillaries are evident, and (C) a plot of normalized OMAG flow signals across the dashed line in (B), corresponding to structural locations marked in (A). In (C), the flow signals (arrows) are ~15μm in size, close to the theoretical OMAG spatial resolution (x-y) of 16 μm.

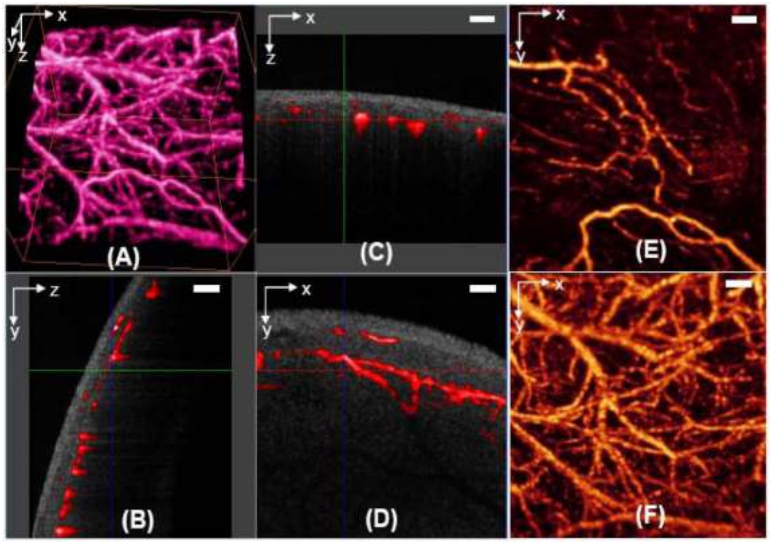

Fig. 4.

A volume of 2.2×2.2×1.7 (x-y-z) mm^3 of an adult mouse brain was imaged with the skull intact, using OMAG. The time to obtain this 3D OMAG image took ~25 s. (A) 3D volumetric rendering of the blood perfusion within the scanned tissue volume. (B), (C) and (D) are the sagittal, coronal, and transverse views of the blood flows fused with the depth-resolved OMAG microstructures within the scanned volume. Using suitable software, this 3-D image can be rotated, cut and examined from any angle to illustrate the spatial relationship between the blood flow and tissue microstructures. (E) and (D) are 2D x-y projection maps showing, respectively, the blood flow within the skull bone and mininges where the blood vessels were less abundant, and the cerebro-vascular flow that maps the detailed blood vessel network, including the capillaries over the cortex. White bar = 200 μm.

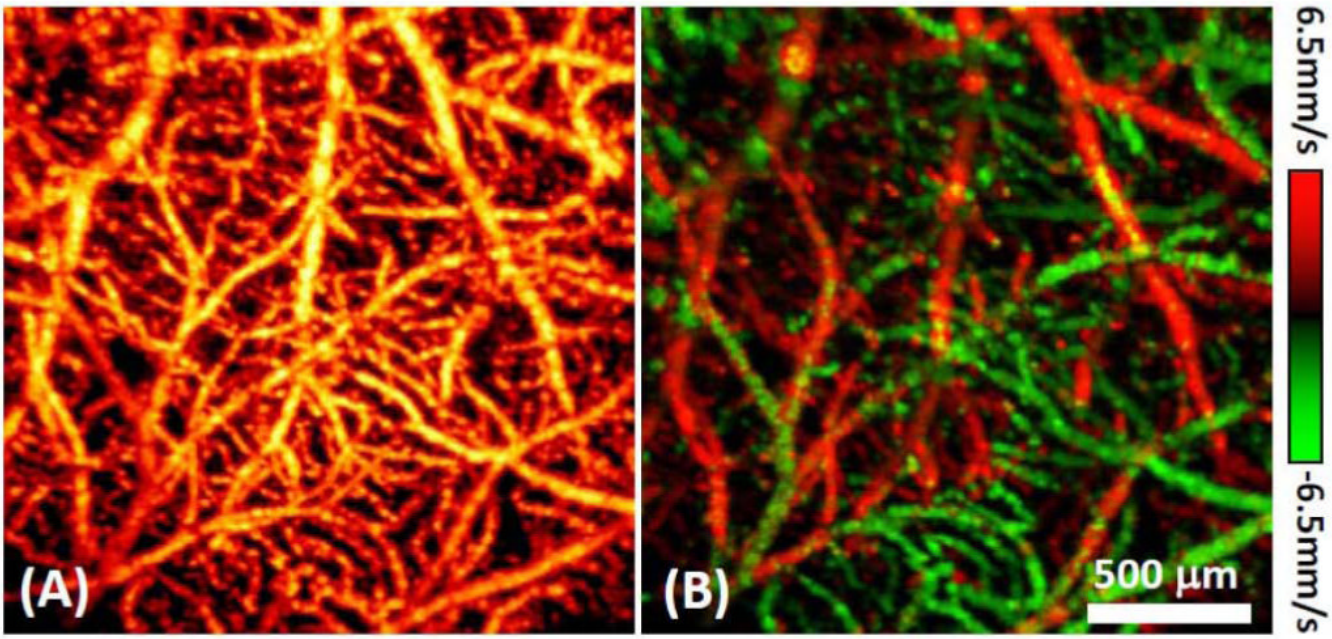

Fig. 5.
(A) OMAG, and (B) DOMAG images of CBF in adult mice under an intact cranium in vivo. The projection images were obtained from a tissue sample volume of 2.2×2.2×2.0 mm^3. Images show superb ability of OMAG and DOMAG to quantify blood flows within scanned tissue.

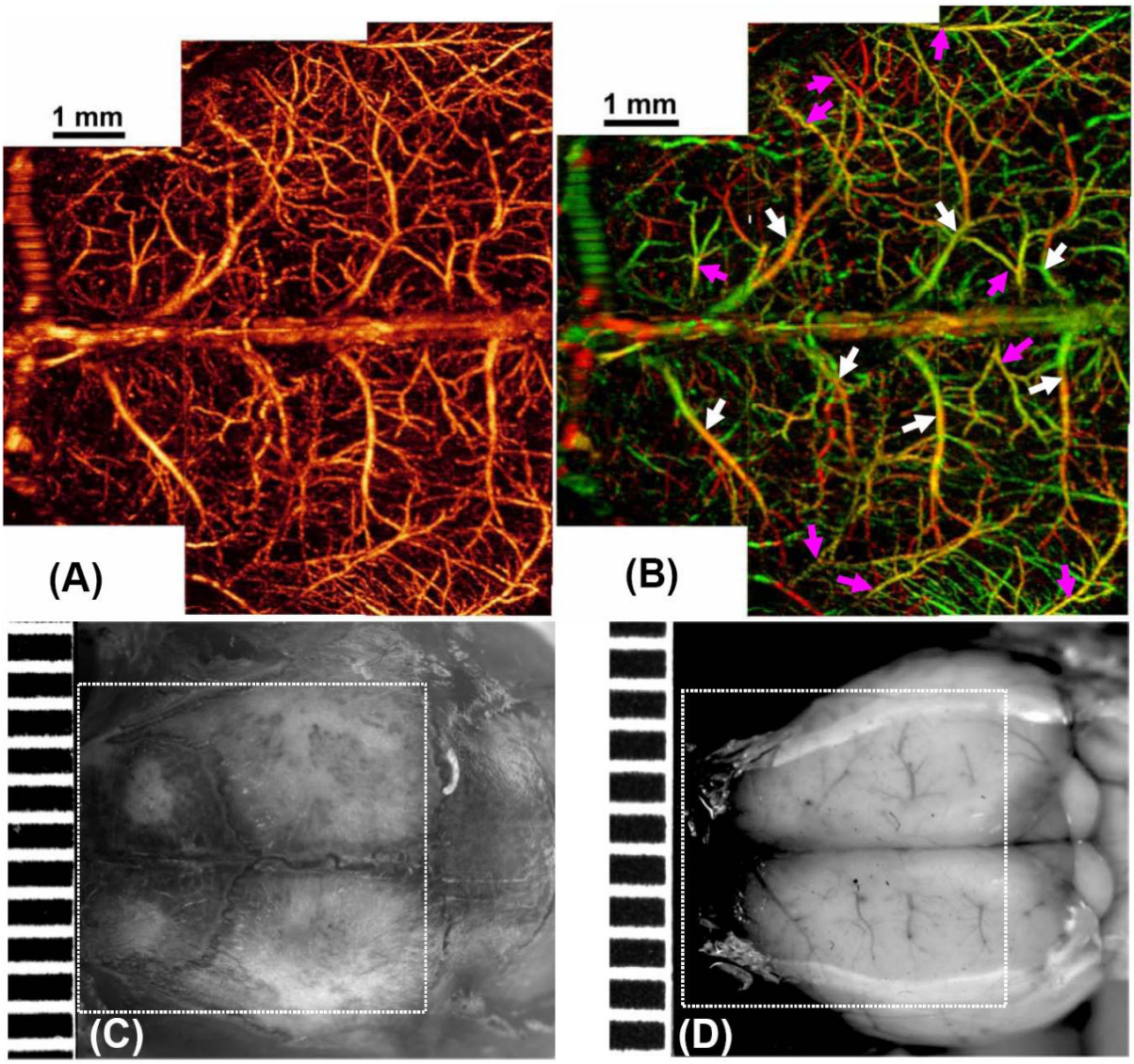

Fig.6.

The cerebral blood flow over the entire cortex of an adult mouse is imaged *in vivo* with the skull left intact. (A) and (B) are the projection views of blood perfusion with and without directional flow information, respectively. With the reference of middle sinus vein, the arteries (pointed by cyan arrows) and veins (white arrows) can be identified in (B). It took ~8 min to acquire the 3D data to obtain (A)/(B) using our current system. The projection image was obtained from OMAG scans of 8 different regions one by one, which were then mosaiced to form (A)/(B). (C) is a photograph of the skull with the skin folded aside where viewing the vasculatures through the skull is impossible. (D) is a photograph showing blood vessels over the cortex after the skull of the same mouse was removed. The superficial blood vessels show excellent correspondence with OMAG images in (A)/(B). The marked white box = 7.5×7.5mm^2

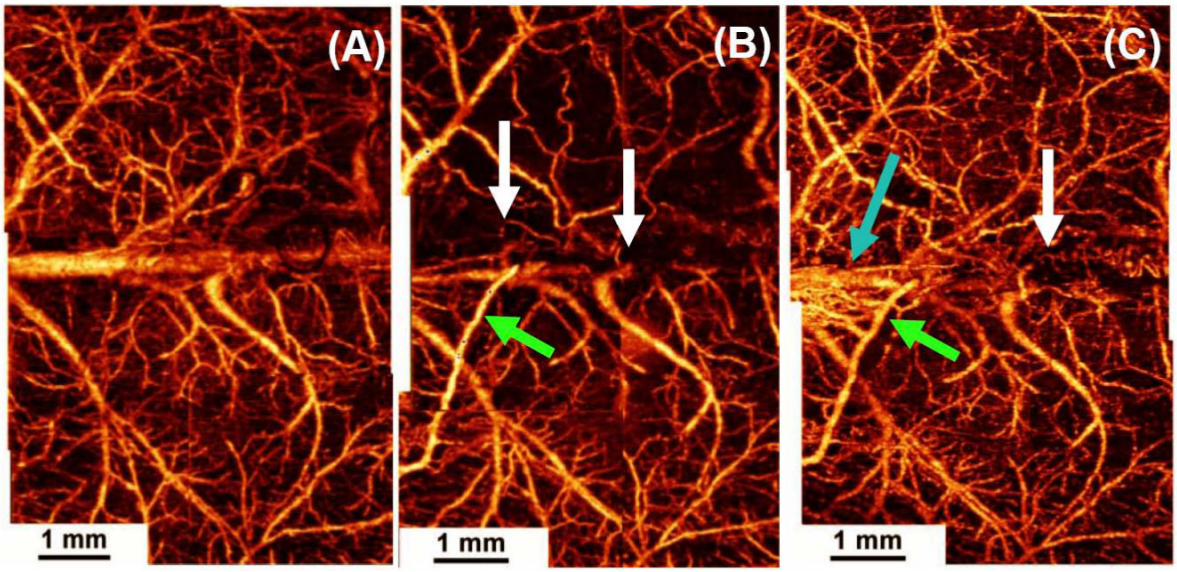

Fig.7.

3D OMAG imaging of the cortex during temporary intraluminal filament-induced MCAO and thrombotic ischemic stroke in mice. Compared to baseline (A), progressive focal occlusion (white arrows) and reorganization of flow patterns (green arrow) develop during MCAO (B), with residual occlusions (white arrow) and increased proximal perfusion (blue arrow) 24 hr later (C). (B) was taken at 60 min into MCAO, and at this point the filament was withdrawn from the MCA.

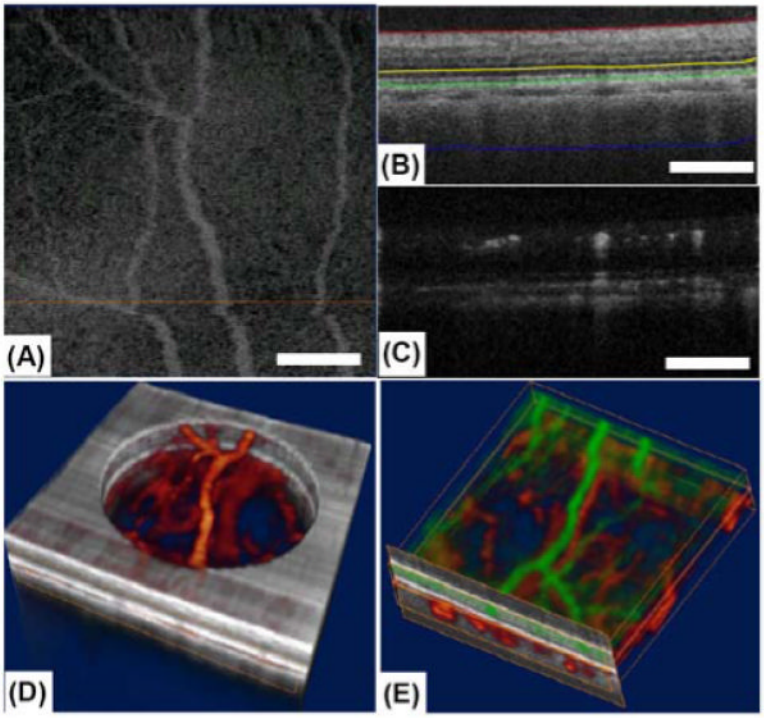

Fig. 8.

In vivo volumetric imaging of posterior chamber of an eye from a volunteer. (A) OCT fundus image of the scanned volume as described in [33]. (B) OCT cross-sectional image at the position marked yellow in (A), in which four lines as shown are resulted from the segmentation method that are used to separate the blood flows in retina and choroids. (C) Corresponding 2D OMAG flow images within the scanned volume. (D) Volumetric rendering of the merged structural and flow images with a cut through in the center of structural image. (E) Volumetric rending of the blood flow image where flows in retina are coded with green and those in choroids with red. Scale bar = 500μm. [15]

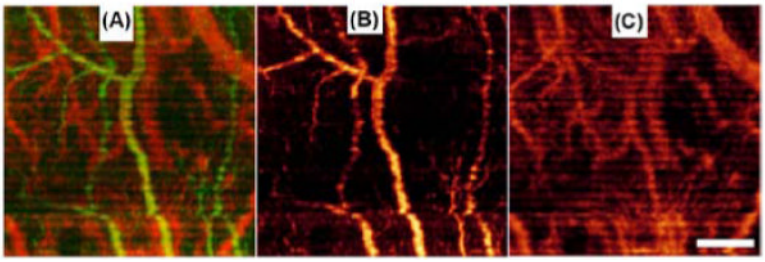

Fig. 9.

x-y projection images from 3D OMAG blood flow images. (A) Projection image from the whole scanned volume with the blood vessels in retina are coded with green color, and those in choroids with red color. (B) x-y projection image from the blood vessels within retina only. (C) x-y projection image from the blood vessels within choroids only. Scale bar = 500μm. [15]